Journal of the Korean Physical Society, Vol. 69, No. 6, September 2016, pp. 903∼908

A New PLS-II In-Vacuum Undulator and Characterization of Undulator Radiation

D-E. Kim, H-H. Lee, K-H. Park, H-S. Seo, T. Ha, Y-G. Jeong,
H-S. Han, W.W. Lee, J-Y. Huang, S. Nam, K-R. Kim and S. Shin*
Pohang Accelerator Laboratory, Pohang University of Science and Technology, Pohang 37673, Korea

(Received 18 November 2015, in final form 8 January 2016)

This paper describes the result of overall studies from development to characterization of undulator radiation. After three years of upgrading, PLS-II has been operating successfully since 21^{st} March 2012. During the upgrade, we developed and installed an in-vacuum undulator (IVU) that generates brilliant X-ray beam. The IVU with a 3 GeV electron beam generates undulator radiation up to $\sim$ 21 keV by using 11^{th} higher harmonic. The characterizations of the undulator radiation at an X-ray beam line in PLS-II agreed well with the simulation. Based on this performance demonstration, the in-vacuum undulator is successfully operating at PLS-II.

PACS numbers: 07.85.Qe
Keywords: Synchrotron radiation, Undulator, X-ray beamline
DOI: 10.3938/jkps.69.903

I. INTRODUCTION

Newer generation light sources with medium electron energy around 3 GeV, as well as the Self Amplified Spontaneous Emission - Free Electron Laser (SASE-FEL) are adopting an In-Vacuum Undulator (IVU) to obtain short-wavelength and high-brilliance X-rays from an undulator with a short magnet period at the required magnetic field. The Pohang Accelerator Laboratory (PAL) [1] developed an IVU during the PLS-II project [2, 3]. With operating experience from the in-vacuum revolver undulator from SPring-8 [4] and the conventional IVU from Advance Design Consulting (ADC) [5] at the Pohang Light Source (PLS) [6], a new IVU with a 20 mm magnetic period and a 1.8 m long undulator length was developed and has been operating in PLS-II.

After completing the design, field shimming and assembly of IVU, we successfully installed and operated an IVU in the PLS-II storage ring. During commissioning of PLS-II, we characterized the undulator radiation at the X-ray scattering beam line in PLS-II. As a result, up to 21 keV undulator radiation was obtained by using 11^{th} harmonic and is available at beamline. Now, a total of 10 IVUs are operating to generate short-wavelength high brilliance X-rays for X-ray scattering, diffraction and nano-imaging studies in PLS-II.

In this paper, we describe the results of overall studies on X-ray characterization from the undulator as well as the IUV development. Section II introduces the overall work to develop the IVU. Section III describes the investigation on their effects on the stored electron beam. The characterization of the IVU radiation at the X-ray scattering beam line is described in Section IV. Finally, Section V presents a summary and concluding remarks.

*E-mail: tlssh@postech.ac.kr

II. DEVELOPMENT OF IN-VACUUM UNDULATOR

A schematic drawing of the IVU is shown in Fig. 1(a), and the main parameters of the IVU are introduced in Table 1. The IVU consists mainly of a mechanical supporter, a magnet array and a vacuum system. The IVU is equipped with online built-in magnetic measurement for the end regions to assess the accuracy of the assembly and the degradation coming from radiation damage or high temperatures.

1. Undulator Design

The designed IVU is a conventional hybrid type undulator, which utilizes ferromagnetic poles to concentrate the magnetic fluxes. The advantage of the hybrid type undulator is that its effective peak field is stronger for the same period as that of the pure permanent magnet type. The performance of a hybrid type insertion device is also known to depend on the mechanical accuracy of the device rather than on the material properties of

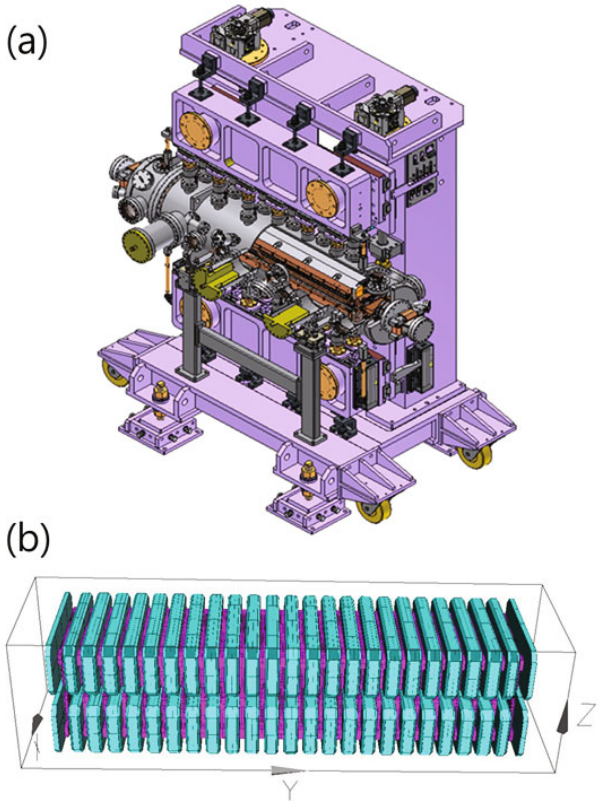

Fig. 1. (Color online) (a) Schematic drawing of the IVU. The IVU consists mainly of a mechanical supporter, a magnet array and a vacuum system. (b) The RADIA model. The dimensions of the chosen magnet is 65 mm (W) × 27 mm (H) × 7.0 mm (T) with 4.0 mm chamfering at the edges. The pole's dimensions are 40 mm (W) × 20 mm (H) × 3.0 mm (T).

the magnet, which are more difficult to control than the mechanical accuracy. The non-uniform magnetization of the permanent magnets has been observed to affect the performance of the undulator, particularly when the gap is small and the electron beam is very close to the magnet. That this kind of local non-uniformity does not show up in the Helmholtz coil measurement, which measures only the total dipole moment of the block, should also be noted.

A Sm_2Co_{17} type rare-earth magnet is selected for the permanent magnet. The remanence of Sm_2Co_{17} ranges between 1.12 T and 1.20 T with a coercivity of 9.8 kOe $\sim$ 11.4 kOe, which is about 10% inferior to the state of the art NdFeB class magnet. Although Sm_2Co_{17} is more brittle and difficult to handle than NdFeB, it has a big advantage in the case of long term radiation damage caused by high energy electron beam irradiation compared to the NdFeB based magnet [7]. Since top-up injection is a default operation mode in PLS-II, beam injection at the minimum operation gap is anticipated, and the long term stability against radiation damage is very important. In addition, Sm_2Co_{17} has a higher Curie

Table 1. Main parameters of the PLS-II in-vacuum undulator.

Parameter	Value	Unit
Undulator type	Hybrid	
Longitudinal symmetry	Anti-symmetric	
Period length	20	mm
Working gap	5.0 $\sim$ 16	mm
Effective field	0.815	T
Magnetic length	1400	mm
Flange-to-flange length	1800	mm
Period number	67	
Magnet material	Sm_2Co_{17}	
Phase error	< 5	Degree
Gap straightness	< 1.0	μm
Vacuum pressure	$<$ 3E-9	Torr

temperature (about 660 °C), and a working temperature with small coefficient of -0.03%/K ($-0.11 \sim -0.12\%$/K for NdFeB). Therefore, it is very safe from the overheating caused by accidental heating during vacuum baking. Moreover, the effect of the temperature increase due to image current heating is minimized. Of course, the magnetic structure is cooled by using a Liquid Cooling Water (LCW) system during baking to protect the magnet's structure from overheating. The LCW system is also used to prevent any drift in the spectrum coming from temperature changes in the magnet's structure due to image current heating. Adoption of Sm_2Co_{17} improves the drift of the spectrum caused by the small temperature drift during the cooling and current cycles. Two coating methods are tested for out-gassing: ion vaper deposit (IVD) coating and Ni coating. The IVD coating was unacceptable; on the other hand, Ni-coating was good enough for the purpose of the IVU. The undulator was assembled using the Ni coating, and no vacuum problems have been caused by the surface outgassing.

The magnetic structure is designed by using RADIA [8], which was developed at European Synchrotron Radiation Facility (ESRF) for insertion device calculation, and cross checked by using ANSYS 3D and OPERA. Due to limited computer resources, only 10 periods of the whole undulator are modelled to assess the periodic part and transition parts. The RADIA model is shown in Fig. 1(b). The magnet dimensions are chosen to be 65 mm (W) × 27 mm (H) × 7.0 mm (T) with 4.0 mm chamfering at the edges. The pole dimensions are 40 mm (W) × 20 mm (H) × 3.0 mm (T). Although the optimum effective peak field was achieved using a thinner pole thickness, a 3.0 mm thickness is chosen due to mechanical considerations. The difference between the optimum and the current configurations was small (about 3%). The longitudinal distribution of the blocks is such that the field is antisymmetric in $z = 0$, which is the undulator's center in the beam's direction. This anti-symmetric

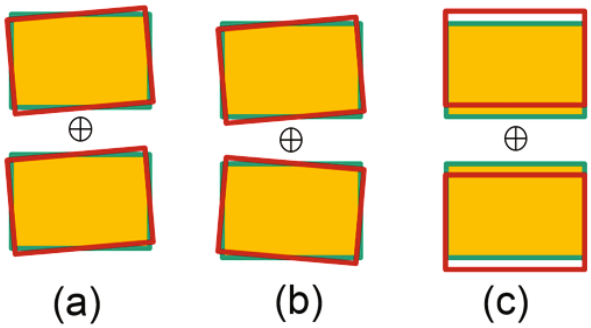

Fig. 2. (Color online) Schematics of pole tuning. (a) This kind of tilting of a pole is used to correct the skew dipole component. (b) This canting of a pole is used to correct the normal quadrupole component. (c) This pole shimming is used to correct the normal dipole component.

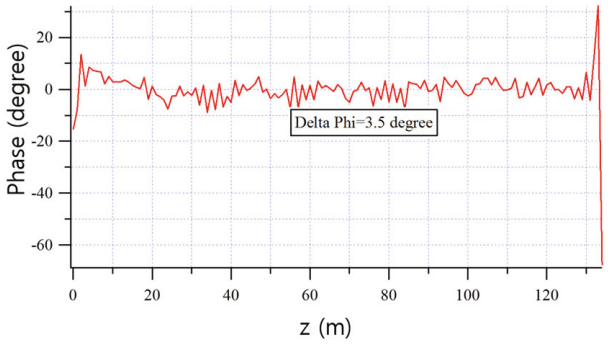

Fig. 3. (Color online) Optical phase errors after final pole tuning. The requirement for an optical phase error excluding transition parts is rms 5 degrees.

configuration has the benefit of a systematic zero 1^{st} field integral for all gaps for ideal materials and geometries. Any deviation from a zero integral is attributed to imperfections in the geometry or the magnetic field, which can be easily tuned to be zero. The weakness of this antisymmetric configuration is that the 2^{nd} field integral is not systematically zero. However, the 2^{nd} integral requirement is weak and can be minimized while designing the transition parts. The transition sequence at the ends is determined by adjusting the space to achieve the periodic field and minimize the 2^{nd} orbit displacement at the end of the undulator. The calculated effective field for a nominal gap of 6.0 mm is 0.815 T. The magnetic length of the undulator is limited to about 1400 mm, resulting in a flange to flange distance of 1800 mm, which is near the maximum installable device length for the short straight section of PLS-II.

2. Field Measurement and Shimming

The assembled undulator is measured and corrected by using a 3-axis hall probe bench. The longitudinal position is measured using a laser interferometer with an accuracy of better than 1 μm. The flatness of the bench is calibrated by using a laser tracker to within 20 μm. The 3-axis hall probe is calibrated for angular error, nonlinearity, and planar Hall effects. The temperature of the entire measurement room is controlled within $\pm$1 K. Also, a flip coil system is used to calibrate the planar Hall effect by measuring the accurate residual field integral. The accuracy of the flip coil system is $\pm$ 5 G·cm.

The undulator is corrected before installing the vacuum chamber. The reproducibility of the undulator assembly was checked by re-measuring the undulator after disassembling the vacuum chamber several times. The assembly is concluded to be sufficiently reproducible.

Pole shimming is carried out by adjusting the pole heights by using copper shims of 10 μm, 30 μm, 50 μm, and 100 μm, as well as combinations of the shims. Pole tuning was conducted in 3 modes as depicted in Fig. 2. Figure 2(a) shows shimming that can correct the skew dipole components and can also correct y-orbits by tilting the vertical magnetic field and by creating a horizontal field. For 3 mrad tilting of a set of upper and lower poles, we can expect about 15.6 G·cm skew dipole corrections. The actual measurement agrees with the calculation within 20%. These corrections at several points along the undulator can straighten the x-orbit, which is needed to improve the optical phase errors. Figure 2(b) shows the correction schemes for normal quadrupole components. By canting a pole, we can adjust the transverse gradient of the residual field integral. For our case of 3 mrad canting of an upper and a lower pole, we can change the integrated normal quadrupole component by 30 G. Figure 2(c) shows the correction scheme for the normal dipole component and the horizontal orbit. This kind of shimming can correct the field amplitude and orbit straightness. The correction is mostly used to minimize the optical phase jitters. After the pole shimming, the optical phase advance per pole becomes uniform, and the average orbit is straight with minimal optical phase errors. The requirement for optical phase error excluding transition parts is 5 degrees rms. The final optical phase errors of the undulators were about 3.5 degrees rms, which satisfies the requirements. Also the ideal spectra with zero beam emittance for the ideal field and the measured field are estimated and compared using B2E code. The calculated spectrum based on the measurement data has achieved 95% of the ideal spectrum at the 5^{th} harmonic.

Figure 3 shows one example of optical phase errors after final pole tuning, and in Fig. 4, the estimated spectrum based on the measured field and the ideal spectrum based on the ideal field are compared. The figure shows that the estimated radiation from the undulator is very close to the ideal one. Here, we considered the 5^{th} harmonic at a 6.0 mm gap with a 3.0 GeV electron beam in the calculation.

The pole tuning described optimized the integrated

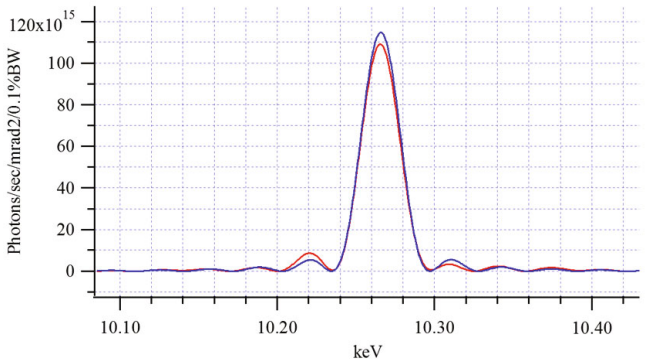

Fig. 4. (Color online) Spectra from an ideal field (blue line) and the measured field (red line). The figure shows that the estimated radiation from the undulator is very close to the ideal one. Here, the 5^{th} harmonic at a 6.0 mm gap with a 3.0 GeV electron beam is considered in the calculation.

Table 2. Main beam parameter changes due to the IVU.

Parameter	Value	Unit
ΔQ_y	0.002	
$\Delta\beta_y/\beta_y$	1.04	%
$\Delta\varepsilon$	0.04	nm rad
$(U-U_0)/U_0$	0.47	%
$(\sigma_E-\sigma_E^0)/\sigma_E^0$	−0.12	%

normal dipole, skew dipole, and normal quadrupole components, and the next few low order integrated multipole errors were corrected using arrays of trim magnets. The smallest unit is a 1.5 mm diameter or a 2.0 mm thick cylindrical shape. Compensation of the field profile is calculated by using RADIA, and the trim magnets are assembled at the end of the undulator. There are three rows in z for each side of trim magnets. One row is used to correct the normal components, the second row is used to correct skew components, and the third row is used for reserve or fine tuning. Using this trim magnet system, the integrated B_x and B_y profiles could be controlled easily and predictably.

III. COMMISSIONING AND OPERATION OF THE IVU

The operation of the IVU in the PLS-II storage ring has brought about several effects that can degrade the overall beam performance. The effects of an IVU on the beam are mainly changes in the beam's parameters, a reduction of the dynamics aperture, a residual orbit distortion, and a vacuum increase in the storage ring. During the PLS-II commissioning, we investigated the effects of the IVU on the beam in the storage ring.

In the storage rings of the recent third-generation light source, insertion devices are placed in the region that has

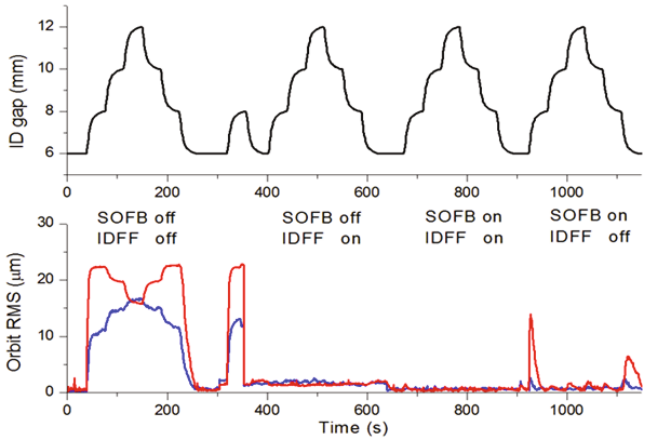

Fig. 5. (Color online) Orbit distortion due to one IVU gap change. ID feed-forward and global orbit correction systems suppress orbit distortion significantly.

finite dispersion, thus affecting beam parameters such as the emittance and the energy spread [9]. The beam-parameter changes are listed in Table 2. Here, the vertical tune shift and the beta-function distortion are caused by the orthogonal component of the magnetic field vertical to the trajectory. The changes in emittance, energy spread, and energy loss are due to undulator radiation. These changes caused by an IVU are less than a few percent, because the peak field and the period length of the undulator are small [10].

The origin of the nonlinearities of the insertion device effects can be critical. The periodic beam path through the insertion device causes nonlinear and periodic magnetic interactions. The effect of the nonlinear intrinsic and transverse field roll-offs from the IVU on particle tracking is very small and negligible due to the small peak field and the period length [10]. However, unlike an ideal insertion device, the first and the second field integrals of the insertion device distort the equilibrium orbit in a real insertion device. The measured rms orbit distortions caused by the IVU in the PLS-II are 1 to 20 for the horizontal plane and 4 to 50 μm for the vertical plane. In order to compensate for the orbit distortion caused by the kick from the IVU, we have introduced an auxiliary steering magnet for insertion-device feed-forward and global orbit correction [11]. This magnet suppresses the orbit distortion y significantly more than a factor of ten, as shown in Fig. 5.

IV. CHARACTERIZATION OF THE IVU RADIATION

1. Theoretical Description

The main purpose of the insertion device is to generate intense synchrotron radiation in the electron storage

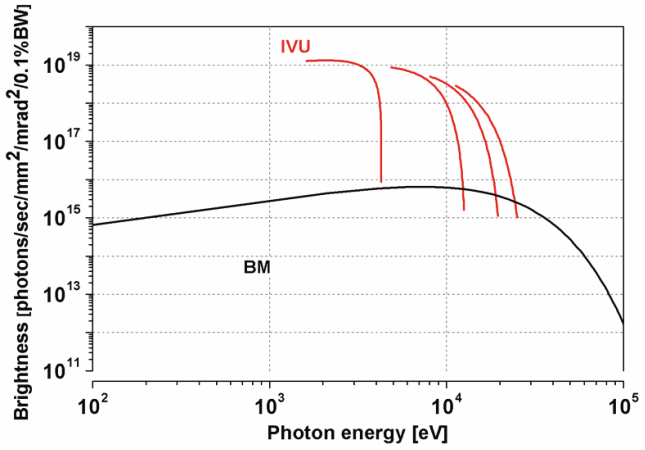

Fig. 6. (Color online) Spectra (in-vacuum undulator vs bending magnet). The spectral brightness of the 1^{st}, 3^{rd}, 5^{th} and 7^{th} harmonics along the IVU's gap are introduced together with the brightness from the bending magnet.

ring. The spectral brightness for a bending magnet and the IVU in PLS-II is shown in Fig. 6. In the figure, the spectral brightness of the 1^{st}, 3^{rd}, 5^{th} and 7^{th} harmonics along the IVU's gap are introduced together with the brightness from the bending magnet. Compared with the radiation from the bending magnet, the spectral brightness of the IVU radiation is 1000 times higher.

The maximum angular deflection of the electron beam in the undulator is much smaller than the opening angle of the radiation cone, and the wavelength radiated from insertion device is

$$\lambda_n(\theta) = \frac{\lambda_w}{2n\gamma^2}\left(1 + \frac{K^2}{2} + \gamma^2\theta^2\right) , \qquad (1)$$

where K is the dimensionless field strength parameter, $n = 1, 2, 3, \ldots$ is harmonic number, λ_w is the undulator magnet period, γ is the relativistic parameter, and θ is radiation observation angle. The spectral width of the peak emission along the beam's axis ($\theta = 0$) is given by

$$\frac{\Delta\lambda}{\lambda} = \frac{1}{nN} , \qquad (2)$$

where N is the number of undulator periods. The linewidth of the undulator is also affected by various factors including the field error and the source size. The source size and the divergence of the radiation from an ideal undulator are given by

$$\sigma_r = \frac{\sqrt{\lambda L}}{2\pi} , \quad \sigma_r' = \sqrt{\frac{\lambda}{L}} , \qquad (3)$$

where L is the undulator length. For a realistic synchrotron light source, the finite beam emittance of the particle beam must be taken into account as well, even when the dominant emittance beam is larger than the diffraction-limited photon beam emittance.

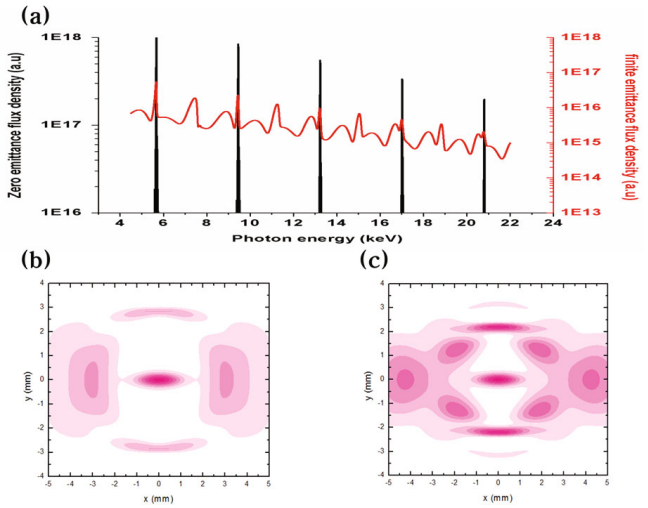

Fig. 7. (Color online) (a) Undulator spectrum of the PLS-II calculated at $K = 1.58$. (b) and (c) are the calculated undulator beam images of the 3^{rd} and the 5^{th} harmonics, respectively.

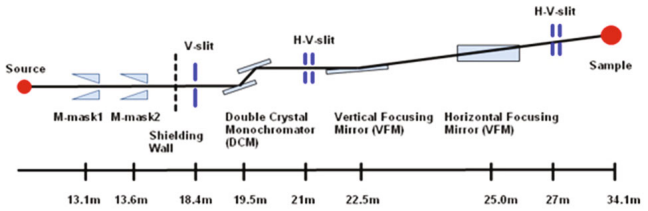

Fig. 8. (Color online) Beamline layout. Optical components of the beamline consist of a double crystal monochromator, a vertical focusing mirror, and a horizontal focusing mirror.

Both the undulator spectrum from zero-emittance and that from finite-emittance electron beams shown in Fig. 7(a) were calculated by using the SPECTRA program. Here, IVU parameters with $K = 1.59$ at $\theta = 0$ are used in the calculation. While the spectrum from the zero-emittance electron beam demonstrates the line character of undulator radiation well, the undulator radiation from the finite-emittance electron beam shows a broad continuous spectrum, including even harmonics due to the spatial effects of undulator radiation. The overall spatial intensity distributions are shown in Figs. 7(b) and (c), including a complex set of different radiation lobes depending on frequency, emission angle, and polarization.

2. Measurement of the IVU Radiation

The 5A XRS BL (X-ray scattering beamline) in PLS-II is dedicated to materials science research. The main scientific programs are in-situ, as well as ex-situ, X-ray scattering experiments on thin films, soft materials, and

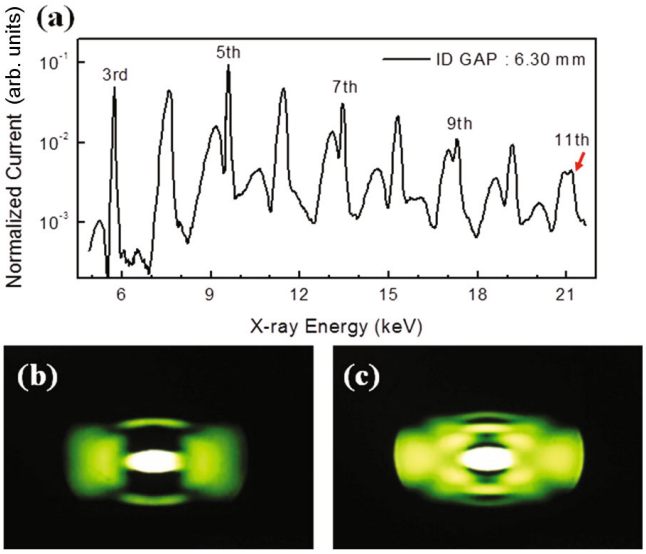

Fig. 9. (Color online) (a) Undulator spectrum of the PLS-II measured at a gap of 6.3 mm. (b) and (c) are the undulator beam images of the 3^{rd} and the 5^{th} harmonics, respectively.

nano-structured materials. The optical layout of the 5A XRS BL is shown in Fig. 8. The optical components consist of a double-crystal monochromator comprised of a pair of Si (111) crystals, a vertical focusing mirror, and a horizontal focusing mirror.

Figure 9 shows the spectrum from the IVU installed for the 5A XRS beamline. The spectrum was measured with the photocurrent from the Cu-plate located after the Si (111) double crystal monochromator. As shown in the figure, the spectra are clear to the 11^{th} harmonics. Due to the limitation of the energy scan range of the double-crystal monochromator, we cannot measure harmonics higher than the 11^{th} harmonic. Figures 9(b) and (c) present images of the harmonics taken at a distance of 20 m from the source with a gap of 6.97 mm. Compared with the simulated images in Figs. 8(b) and (c), the measured images indicate the central cone very clearly while the other structures are symmetric. This directly ensures that the devices are developed as they were designed.

V. SUMMARY

In this paper, we introduced a new IVU designed and developed for an X-ray source at PLS-II. Their effects on the beam operation were also described, and its effect on beam operation was found to be negligible or suppressible. The characterizations of the undulator radiation at an X-ray beam line in PLS-II agreed well with the simulation. Based on this performance demonstration, the IVU is successfully operating at PLS-II.

ACKNOWLEDGMENTS

We would like to thank H. Wiedemann for useful discussions and guidance. This research was supported by the Converging Research Center Program through the Ministry of Science, ICT and Future Planning, Korea (NRF-2014M3C 1A8048817) and the Basic Science Research Program through the National Research Foundation of Korea (NRF-2015R1D1A1A01060049).

REFERENCES

[1] Pohang Accelerator Laboratory: http://pal.postech.ac.kr/.
[2] S. Nam, *Major Upgrade Activity of the PLS in PAL: PLS-II*, PAC, Vancouver, Canada, 4 May 2009, TH4PBC03.
[3] S. Shin *et al.*, J. Instrum. **8**, P01019 (2013).
[4] T. Hara, Nucl. Instr. and Meth. A **467**, 161 (2001).
[5] A. Deyhim, *Development of accurate and precise in-vacuum undulator system*, PAC, New York, NY, USA (2011).
[6] M. Yoon and T. Lee, Rev. Sci. Instrum. **68**, 2651 (1997).
[7] T. Bizen, AIP Conference Proceedings **705**, 167 (2004).
[8] O. Chubar, J. Syn. Rad. **5**, 481 (1998).
[9] J. Corbett *et al.*, Effect of insertioin devices in SPEAR3, PAC, New York, NY, USA (1999).
[10] S. Chunjarean, D-E. Kim and S. Shin, J. Korean Phys. Soc. **64**, 1259 (2014).
[11] C. Kim, J. Hou, H. Kang, I. Hwang, E. Lee, S. Shin, S. Park, K. Kim and S. H. Nam, J. Korean Phys. Soc. **59**, 34 (2011).